Hydrology Research

British Hydrological Society

IWA PUBLISHING



Hydrology Research Vol 52 No 5, 1048 doi: 10.2166/nh.2021.188

# Accuracy assessment and error cause analysis of GPM (V06) in Xiangjiang river catchment

Bingru Tian[a], Hua Chen [a,*], Jialing Wang[a,b] and Chong-Yu Xu [c]

[a] State Key Laboratory of Water Resources and Hydropower Engineering Science, Wuhan University, Wuhan 430072, China
[b] Changjiang Survey, Planning, Design and Research Co., Ltd, Wuhan, China
[c] Department of Geosciences, University of Oslo, Oslo, Norway
*Corresponding author. E-mail: chua@whu.edu.cn

HC, 0000-0002-2320-3228

## ABSTRACT

Application potential and development prospect of satellite precipitation products such as Tropical Rainfall Measuring Mission (TRMM) and Global Precipitation Mission (GPM) have promising implications. This study discusses causes of spatiotemporal differences on GPM data through the following steps: Initially, calculate bias between satellite-based data and rain gauge data of Xiangjiang river catchment to assess the accuracy of GPM (06E, 06 L, and 06F) products. Second, total errors of satellite precipitation data are divided into hit bias (HBIAS: precipitation detected by both GPM and rain gauge station), missed precipitation (MBIAS: precipitation detected only by rain gauge station), and false precipitation (FBIAS: precipitation detected only by GPM). Third, evaluate the impact of precipitation intensity and total precipitation on accuracy of GPM data and their influence on three error components. Several conclusions are drawn from the results above. (1) Satellite-based precipitation measurements perform better on a larger temporal-spatial scale. (2) The accuracy of TRMM and GPM data displays significant variances on space and time. Season, precipitation intensity, and total precipitation are main factors influencing the accuracy of TRMM and GPM data. (3) The detection capability of satellite products change with seasonal variation and different precipitation intensity level.

**Key words:** accuracy assessment, error components, extreme events, precipitation intensity, satellite measurements

## HIGHLIGHTS

- GPM products have wider spatial coverage, higher temporal and spatial resolution than TRMM products.
- GPM products are more in line with the data requirements of hydrological simulation and forecast.
- Evaluate accuracy of different GPM products in precipitation measuring, including early, late and final products.
- Assess the improvement of GPM products comparing with its predecessor, TRMM.

## 1. INTRODUCTION

As a basic element of hydrology and meteorology, precipitation is a vital segment in the global water and energy circle. Rainfall amount and spatiotemporal distribution information are the basis of hydrological analysis. Precipitation also directly affects hydrological simulation since it is a driving variable of the rainfall–runoff process, in addition, accuracy of precipitation spatiotemporal distribution can determine the following aspects: fresh water resources deployment and management, industrial and agricultural production and development, ecological balance and environmental protection, meteorology and climate forecast applications, and so on. Additionally, extreme precipitation events directly affect drought and flood disaster prevention and management. All of those aspects are closely related to human life, especially social and economic development. Despite precipitation playing a vital role in many areas, it is still a great challenge to obtain accurate and reliable precipitation information due to not only uneven distribution of precipitation but also complex evolution along space and time (Mishra & Coulibaly 2009).

However, acquisition methods of precipitation data are becoming more diverse at present, with the main measurement methods including ground-based radar measurement, satellite-based rain measurement, and rain gauge stations (Huffman

*et al.* 2010). Among these methods, the traditional observation method (rain gauge) is usually recognized as a relatively accurate method of rain measurement in hydrology and is the most common source of current hydro-meteorological precipitation data. The technology of rain gauges is mature and has been in widespread use for a long time. While high-quality precipitation datasets can be obtained at station points, precipitation observed by rain gauge is distributed in discrete points and rainfall data in relation to surrounding area still need to be obtained by interpolation (Camera *et al.* 2014; Lopez *et al.* 2015). As a consequence, rain gauge measurements have limitations in obtaining an accurate spatiotemporal distribution of precipitation. The absence of precipitation data is particularly acute in complex terrain with sparsely populated areas or ocean areas. Radar-based precipitation measurements have been proposed and gradually popularized as auxiliary rainfall measurements (Sauvageot 1994; Meischner *et al.* 1997; Krajewski & Smith 2002). However, radar-based rainfall measurements are also limited by many factors, such as size and distribution of raindrop, obstacle block and snowmelt, and these external elements will produce interference to radar signals (Germann *et al.* 2010). As well, the high cost of radar products in installation and maintenance are also a reason for its relatively narrow application range in hydrology.

In recent years, satellite remote sensing technology has emerged (Kidd 2010) and been applied in different fields such as meteorology, oceanography, and hydrology. Current launched polar-orbiting satellites and geostationary satellite groups have formed global coverage. A variety of multisatellite precipitation products have been released and have received extensive attention all over the world (Ebert *et al.* 2007; Pari *et al.* 2013), such as Tropical Satellite Rainfall Measurement Mission (TRMM) and its next generation, Global Precipitation Measurement Mission (GPM). Remote sensing satellite products have wide range coverage and a good spatial and temporal resolution. Therefore, satellite-based precipitation measurement is a good application prospect in areas where hydrological data are deficient and it has become popular worldwide. Since satellite-based precipitation measurements are relatively new methods, the accuracy of satellite-based measurements needs to be widely verified due to their various sensor information sources and inversion algorithms. At the same time, there is still a certain bias between satellite-based precipitation products and rain gauge precipitation data on the ground. Thus, in-depth analysis of error and cause analysis of precision variation is still a key research topic at present.

As typical satellite precipitation products, many studies have researched and assessed TRMM and GPM precipitation products. Most of these studies have used ground-based observations to verify data accuracy. Some of them have pointed out that the TMPA research products (3B42 V6 and V7) perform better than their real-time counterparts (RTV6 and RTV7) because they use monthly gauged dataset to amend data (Wang *et al.* 2018). The later version, V7, performs better than the previous V6 because of an improved algorithm and updated data inputs (Chen *et al.* 2013a, 2013b; Zulkafli *et al.* 2014). Based on preceding studies, uncertainty of satellite measurements is more or less related to latitude, topography, and climate (Yong *et al.* 2016). In addition, misestimating (either overestimation or underestimation) of TRMM precipitation varies from region to region (Zhang *et al.* 2011; Cai *et al.* 2015). As for the precipitation intensity, most studies (Chen *et al.* 2013a, 2013b; Adam *et al.* 2015; Pipunic *et al.* 2015) found that satellite products have a tendency to overmeasure low precipitation but undermeasure high precipitation. Some studies use data assimilation methods to reduce bias between ground-based and satellite-based precipitation (Adam *et al.* 2015). To analyze errors embedded in the satellite precipitation products, a methodology to decompose data errors has been proposed: some studies state that the amplitude of each error component is larger than total errors because there is a mutual cancellation among error components (Chen *et al.* 2013a, 2013b). This method has been adopted to estimate satellite-based precipitation error over different climate regimes and some studies found that regional and seasonal diversity cause significant differences in the error components (Yong *et al.* 2016). Otherwise, there are still some problems worthy of attention and exploration. First, accuracy evaluation is not systematic enough: there are some limitations, for example, data are not up to date, evaluation indexes tend to be simple, duration of study tends to be short, and so on. Second, in order to verify the improvement of GPM compared with TRMM and figure out influence factors that cause bias, error sources of GPM need to be analyzed synthetically, so as to provide a valuable reference for data and algorithm development for further improvement. Hence, it is necessary to evaluate satellite-based precipitation data systematically.

For the above reasons, three main research objectives in this study are proposed: the first purpose is to measure spatiotemporal difference and evaluate the accuracy of satellite precipitation measurements; then to figure out error sources and causes of those differences; the final objective is to further improve the accuracy of satellite precipitation data based on the above study and apply in hydrological simulation. The objects of this study are TRMM and GPM products. The research area is Xiangjiang river catchment with relatively dense and uniform distributed rain gauges, selected to carry out the study of accuracy evaluation, error and cause analysis. The structure of this paper is as follows. Section 2 briefly introduces the study area

and data sources. Section 3 gives a short explanation of data evaluation methodology. Then, the following section mainly presents the calculated results and some discussion of the results. Finally, section 5 concludes with the major results of this study.

## 2. STUDY AREA AND DATA SOURCES

### 2.1. Study area

Xiangjiang River is one of the main tributaries of the Yangtze River. It originates in Lingui, Guangxi Autonomous Region, flows through Hunan Province, and drains into Dongting Lake (Wang *et al.* 2018). The Xiangjiang river catchment, the area of which is 94,660 km², is located in southern China, and lies in between 24°31′N–29°00′N and 110°31′E-114°00′E (Figure 1). The climate of the region is humid subtropical monsoon type with annual mean temperature higher than 17 °C and average annual precipitation of above 1,500 mm. The main water sources of Xiangjiang River and its tributaries are rainfall; therefore, duration and intensity of precipitation play important roles in Xiangjiang river flow. The temporal distribution of precipitation is uneven and most precipitation occurs between April and September. The east, south, and west sides of catchment are surrounded by mountains while other landforms are undulating hills and river plains. Complexity of the catchment topography results in the acceleration of runoff.

### 2.2. Rain gauge data

This study uses observed daily precipitation data from the high-density rain gauge network over the Xiangjiang river catchment area as a reference for the evaluation of satellite rainfall products. Due to the termination of the TRMM product in 2014, when evaluating different satellite rainfall products, the time range of data is slightly different: 226 rain gauges daily data from 2006 to 2014 are chosen to evaluate TRMM products (3B42 V7), while daily data from 2006 to 2018 at the same rain gauges are selected to compare with GPM data. Data source of rain gauges are collected from the hydrological almanac of Dongting Lake District provided by Hydrologic Office of Hunan Province, which is reliable and strictly quality controlled.

Both TRMM and GPM data are raster data, but rain gauge data are discrete data with point distribution. Therefore, in order to process the original rain gauge data into grid rainfall data with the same scale as satellite data, this study uses the ordinary

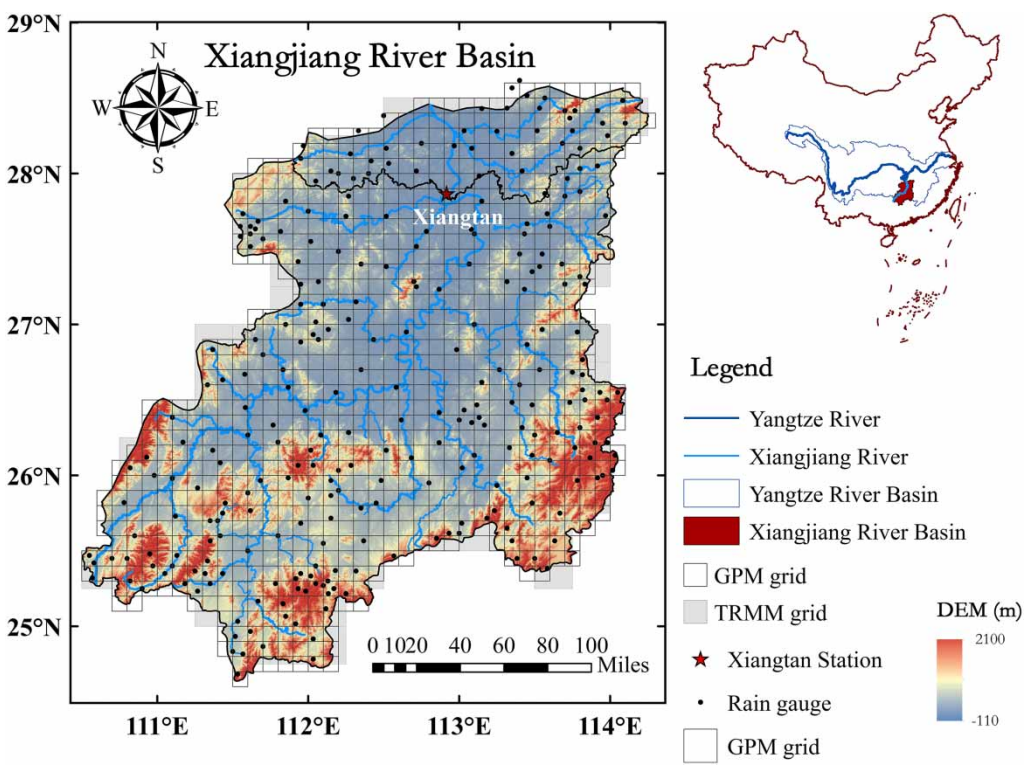


**Figure 1** | Location of rain gauges and distribution of GPM grids in Xiangjiang river catchment.

kriging (OK) method (Krige 1951) to raster the gauge data in ArcGIS. Based on different rainfall characteristics, this geostatistical method identifies a suitable variogram model to optimize the rain gauge network (Foehn *et al.* 2018). Finding an optimum of the appropriate number and location of stations which produce the minimum kriging error can achieve the optimal network configuration (Adhikary *et al.* 2015). Briefly, precipitation interpolation based on the OK method uses observed data of the surrounding rainfall stations to calculate values of the unsampled points. According to the spatial location of rainfall stations and the correlation between each observed data, corresponding weights are assigned to data from rain gauge stations. For the OK method, the weight coefficient satisfies two conditions: (1) the minimum estimation variance and (2) the unbiased estimation (Ly *et al.* 2011). A general expression of kriging method is as follows (Adhikary *et al.* 2015):

$$Z(x_0) = \sum_{i}^{n} \lambda_i Z(x_i) \tag{1}$$

where $Z(x_0)$ is the interpolated estimate of $Z$ at $x_0$ point and $Z(x_i)$ is the observed data at $x_i$; $\lambda_i$ represents weights that satisfy the above conditions; $n$ is the total number of observations.

Some studies have revealed that the OK method is an efficient way for the interpolation of daily precipitation and have shown that the difference between interpolation methods decreases as the density of rain gauge stations increases (Basistha *et al.* 2008; Ly *et al.* 2011; Haggag *et al.* 2016). Therefore, this study uses the OK method to interpolate the gauge data to a grid of 1 km × 1 km and then calculates the grid average rainfall according to the required spatial resolution.

### 2.3. TRMM data

TRMM is a satellite mission used as a tropical and subtropical precipitation measurement. The US National Aeronautics, Space Administration (NASA) and Japan's Aerospace Exploration Agency (JAXA) co-sponsored the TRMM project until the termination of the TRMM product in 2014. Data source is available on the following website (https://pmm.nasa.gov/data-access/downloads/trmm). Daily precipitation data from 2006 to 2014 are derived from the TMPA product (3B42 V7). Spatial resolution of this 3-hourly satellite precipitation product is 0.25° × 0.25°. In this paper, there are 140 TRMM pixels covering the study area.

### 2.4. GPM data

As can be seen on the NASA website, in earlier versions, GPM datasets are computed for the GPM era, starting in March 2014. Now, the GPM datasets use TRMM as a calibrator for the period from the start of TRMM observations to several months after the launch of the GPM Core Observatory to allow GPM processing spin up and a graceful transition from the TRMM era to the GPM era. Therefore, GPM data are assessed by using three products of IMERGE during the research period (2006–2018). They are two real-time products 06Early, 06Late with different delay in version 06 and a version of research product 06Final, respectively. GPM rainfall data can be downloaded on NARS official website (https://pmm.nasa.gov/data-access/downloads/gpm), where the details of GPM products 06Early, 06Late, and 06Final are provided. Precipitation data are obtained with a 0.5 h temporal resolution and 0.1° × 0.1° spatial resolution. A total of 909-GPM pixels are able to cover the whole study area (Xiangjiang river catchment).

### 2.5. Other data

Other data include topographic data, land use and soil texture information, and meteorological data. DEM data used in this study were downloaded from the geospatial data cloud website of computer network information center of Chinese Academy of Sciences (http://www.gscloud.cn). Its spatial resolution is 30 m. When used, the nearest neighbor method is adopted to resample the elevation data into the spatial resolution consistent with the satellite grid data, which is used to represent the average elevation of each grid. Table 1 is a detailed description of the source and processing of the main data.

## 3. METHODOLOGY

### 3.1. Accuracy evaluation of precipitation estimation

In order to evaluate the precision of rainfall estimation of satellite precipitation products, eight quantitative estimation indices were introduced (see Table 2). Linear correlation coefficient (CC) and Nash–Sutcliffe efficiency coefficient (NSE) reflect consistency degree of satellite data and ground-verified (GV) data. Mean error (ME), mean absolute error (MAE), and root mean

**Table 1** | Data source description

| Data | Type | Description | Resolution | Time duration | Source from |
|---|---|---|---|---|---|
| Hydrological data | Precipitation<br>Evaporation<br>Runoff | 226 rain gauges<br>12 stations<br>Xiangtan station | Day | 2006–2018 | Hydrologic Data Year Book |
| Satellite precipitation data | TMPA<br>IMERGE<br>IMERGE<br>IMERGE | 3B42 V7<br>06 V Early run<br>06 V Late run<br>06 V Final run | 3 h/0.25°<br>0.5 h/0.1° | 2006–2014<br>2006–2018 | NASA<br>NASA |
| Meteorological data | Wind speed<br>Temperature<br>Solar duration<br>Relative humidity | 13 weather stations | Day | 2006–2018 | National Meteorological Information Centre |
| Basic geographic data | DEM | ASTER GDEM | 30 m | 2009 | GSCloud |

**Table 2** | Evaluation indices

| Indices | Equations | Name |
|---|---|---|
| CC | $CC = \frac{\sum_{i=1}^{n}(S_i - \bar{S})(G_i - \bar{G})}{\sqrt{\sum_{i=1}^{n}(S_i - \bar{S})^2}\sqrt{\sum_{i=1}^{n}(G_i - \bar{G})^2}}$ | Correlation coefficient |
| NSE | $NSE = 1 - \frac{\sum_{i=1}^{n}(S_i - \bar{G})^2}{\sum_{i=1}^{n}(G_i - \bar{G})^2}$ | Nash efficiency coefficient |
| ME | $ME = \frac{1}{n}\sum_{i=1}^{n}(S_i - G_i)$ | Mean error |
| MAE | $MAE = \frac{1}{n}\sum_{i=1}^{n}\lvert S_i - G_i\rvert$ | Mean absolute error |
| RMSE | $RMSE = \sqrt{\frac{1}{n}\sum_{i=1}^{n}(S_i - G_i)^2}$ | Root mean square error |
| RE | $RE = \frac{\frac{1}{n}\sum_{i=1}^{n}(S_i - G_i)}{\bar{G}} \times 100\% = \frac{\sum_{i=1}^{n}(S_i - G_i)}{\sum_{i=1}^{n} G_i} \times 100\%$ | Relative error |
| NMAE | $NMAE = \frac{\frac{1}{n}\sum_{i=1}^{n}\lvert S_i - G_i\rvert}{\bar{G}} \times 100\%$ | Normalized mean absolute error |
| NRMSE | $NRMSE = \frac{\sqrt{\frac{1}{n}\sum_{i=1}^{n}(S_i - G_i)^2}}{\bar{G}} \times 100\%$ | Normalized root mean square error |

$n$ is sequence length, $S_i$ and $G_i$ are satellite precipitation data and rain gauge data, respectively, while $i$ is the number of data point; $\bar{S}$ and $\bar{G}$ are mean value of satellite precipitation data and gauge data, respectively.

square error (RMSE) characterize deviation magnitude of satellite data compared with GV data. The relative quantities corresponding to these three indexes are taken (relative error RE, normalization absolute error RMAE, and normalized root mean square error NRMSE) to evaluate relative deviation between satellite data and GV data.

### 3.2. Capability of rainfall event detection

A verification method (verification of two-variable prediction contingency table, see Table 3) generally employed in weather forecast verification was applied to investigate the accuracy of satellite rainfall products in detecting rainfall events. Referring to some studies (Tian *et al.* 2009; Moazami *et al.* 2013), 1 mm/d was used as the daily rainfall threshold. Generally, that is, when precipitation is greater than or equal to 1 mm/d, it is considered as a precipitation event, and if it is less than the threshold, it is considered as no rain. Actual rainfall status is based on rain gauge data, when there is rain, recording as '1' otherwise recording as '0'. Consequently, four scenarios arise:

1. The satellite-based products and rain gauge detected rain at the same time;
2. Satellite-based products captured rain, conversely, GV data showed no rain;
3. Satellite-based products indicated no rain but GV data showed the opposite situation;
4. Neither the satellite-based products nor rain gauge detected precipitation events.

According to these scenarios, probability of detection (POD), false alarm ratio (FAR), and Heidke skill score (HSS) are applied to appraise the capability of satellite-based products in capturing rainfall events (Equations (2)–(4)). To clarify, HSS denotes the comprehensive ability of satellite products to capture rainfall events (Wilks 2006; Hyvarinen 2013).

$$POD = \frac{n_{11}}{n_{11} + n_{01}} \tag{2}$$

$$FAR = \frac{n_{10}}{n_{11} + n_{10}} \tag{3}$$

$$HSS = \frac{2(n_{11}n_{00} - n_{10}n_{01})}{[(n_{11} + n_{01})(n_{01} + n_{00}) + (n_{11} + n_{10})(n_{10} + n_{00})]} \tag{4}$$

where $n_{11}$, $n_{01}$, $n_{10}$, and $n_{00}$ are number of occurred hit error, missed precipitation, false precipitation, and no rain event.

### 3.3. Ability of extreme precipitation estimate

Extreme events have significant impacts on social economy, life safety, and ecological environment because extreme rainfall events directly affect the occurrence and intensity of drought or flood events. This paper assesses the capacity of satellite precipitation products to estimate extreme rainfall through three aspects: the magnitude, the occurrence time, and the duration of extreme rainfall events. A series of indices known as the Expert Team on Climate Change Detection and Indices (ETCCDI) has been defined. This study chooses five criteria (Dp20, CDD, CWD, P1d, P5d) based on ETCCDI. In addition, other criteria including extremely wet days (P99), when the maximum 1-day precipitation occurred in the year (Day1) and the middle day of when the maximum 5-day precipitation happened in the year (Day5) are considered as well. In total, eight indices are selected to assess the ability of satellite precipitation products analyzing extreme events (see Table 4).

**Table 3** | Crosstab of the comparison between satellite-based precipitation data and ground rain gauged data

| | Ground verification data (GV) | |
|---|---|---|
| **Satellite-based data (S)** | **1** | **0** |
| 1 | n11 (hit) | n10 (false) |
| 0 | n01 (miss) | n00 |

The symbols n11, n10, n01, n00 represent hit, false, missed, and no rain precipitation events, respectively.

**Table 4** | Criteria of extreme precipitation estimation

| Index | Index name | Indicator definitions | Unit |
|---|---|---|---|
| Dp20 | Number of very heavy precipitation days | Annual count when precipitation ≥20 mm | d |
| CDD | Consecutive dry days | Maximum continuous days when precipitation ≤1 mm | d |
| CWD | Consecutive wet days | Maximum continuous days when precipitation ≥1 mm | d |
| P1d | Max 1-day precipitation | Maximum 1-day precipitation | mm/d |
| P5d | Max 5-day precipitation | Maximum 5-day precipitation | mm |
| P99 | Extremely wet days | Annual total precipitation from days >99th percentile | mm/d |
| Day1 | | The max 1-day precipitation day of the year | – |
| Day5 | | Middle of the maximum 5-day precipitation day of the year | – |

### 3.4. Error decomposition

Precipitation estimation error is the difference between satellite precipitation data and GV data. Error decomposition aims at a further exploration of compositions and sources of error. According to the two main steps of satellite precipitation measuring, total error of satellite precipitation estimation is divided into three components (Tian *et al.* 2009); the relationship between the three error components and the total error can be expressed as:

$$TBIAS = \sum_{i=1}^{n_{11}} hbias + \sum_{j=1}^{n_{01}} mbias + \sum_{k=1}^{n_{10}} fbias = HBIAS + MBIAS + FBIAS \quad (5)$$

where *TBIAS* is total bias of precipitation; *hbias* is hit error, *mbias* is missed precipitation, and *fbias* is false precipitation. The corresponding space–time accumulations of the three biases are *HBIAS*, *MBIAS*, and *FBIAS*, respectively; $n_{11}$, $n_{01}$, and $n_{10}$ are number of times of hit error, missed precipitation, and false precipitation event have occurred; $i$, $j$, and $k$ represent order of the precipitation event.

## 4. RESULTS AND DISCUSSION

### 4.1. Accuracy assessment of satellite-based precipitation estimates

#### 4.1.1. Capability of depicting rainfall spatiotemporal distribution

Accuracy assessment of satellite precipitation products in this paper is based on the comparison with GV data. The research period of TRMM was 2006–2014 and that of GPM 2006–2018. Spatial distribution of annual rainfall reflected the ability of satellite products to describe spatial and temporal distribution characteristics of precipitation. Figure 2 demonstrates that both TRMM and GPM products (06E, 06 L, 06F) can give a general description of rainfall process. Figure 2(b) illustrates the difference of annual rainfall between GPM data and GV data: rainfall is prone to significant underestimate by GPM products, especially research product (06F). Nevertheless, the spatial distribution of precipitation estimated by research product (06F) resembled more the GV data contrasting with the real-time products (06E, 06 L).

Figure 2(a) presents the average annual precipitation distribution from 2006 to 2014 based on rain gauge-verified data and TRMM data qualitatively. As can be seen, TRMM data and GV data show a quite similar trend. There is a larger amount of precipitation in the northeast and southwest of the catchment but less precipitation in the western and central parts of the study region. Figure 2(a) reveals a gradual falling of precipitation from southeast and southwest to inland. This is mainly due to a combination of climatic and topographic factors. In general, TRMM data tend to underestimate at different geographic locations in the catchment except the southwest corner area.

Compared with TRMM data, GPM data are able to display a more specific precipitation distribution due to their higher resolution in space. Similar to TRMM data, Figure 2(b) demonstrates that GPM precipitation data also show a decreasing trend from the southwest and northeast to the middle of the Xiangjiang river catchment. However, different from the overall tendency to underestimate rainfall of TRMM, GPM products tend to underestimate precipitation in heavy rainfall regions but overestimate in the center of the catchment with relatively low rainfall. On the other hand, comparing the precipitation

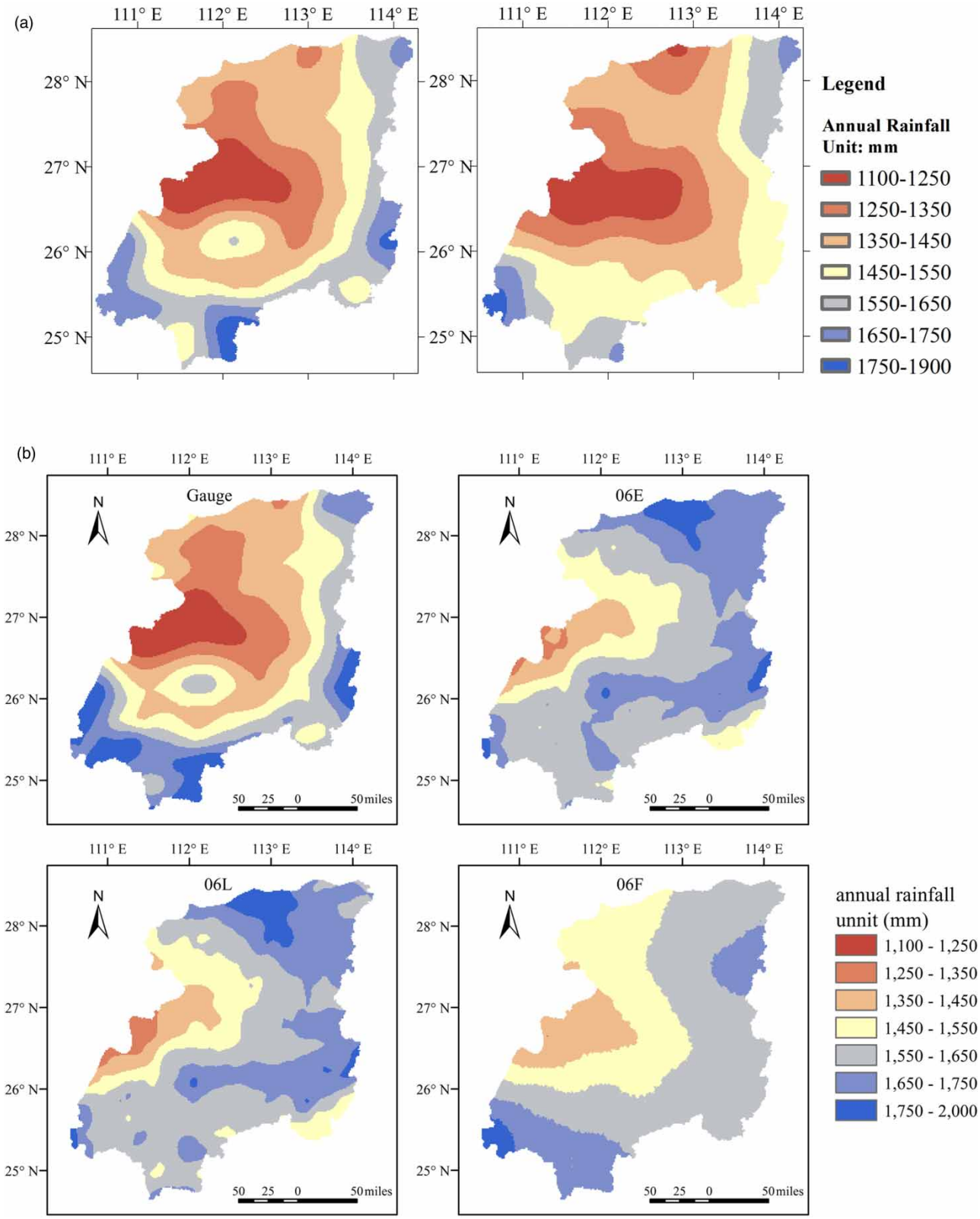


**Figure 2** | Spatial distribution of accumulated rainfall for: (a) TRMM and the rain gauge data over 2006–2014 (Wang *et al.* 2018) and (b) GV data and four GPM products' data during 2006–2018.

distribution of three GPM products and rain gauge in Figure 2(b), it can be seen that the overestimation of precipitation in the northeast region and the underestimation of precipitation in the southwest region of GPM real-time products have been improved after post-processing. Thus, compared with real-time product 06E and 06 L, the research product 06F data was closer to GV data in describing the trend of precipitation spatial distribution.

In summary, with the development of technology, satellite rainfall products have a higher spatial and temporal resolution, which indicates the rainfall estimation capability of satellites is gradually improving. Under large spatial scale conditions, GPM products can roughly depict precipitation distribution in space, and the following text will further verify their accuracy of precipitation estimation.

#### 4.1.2. Evaluation of GPM data under different spatial scale

Table 5 indicates evaluation results of three sets of GPM products during the period from 2006 to 2018, compared to TRMM results calculated by Wang *et al.* (2018).

The accuracy of satellite precipitation data is evaluated by quantitative calculation of statistical indices from different scales. The capture capacity of satellite rainfall data for rainfall events is reflected from probability of detection (POD), false alarm ratio (FAR), and Heidke skill score (HSS). Table 5 illustrates the results of statistical indices. CC value of research product 06F is 0.78 while CC values of real-time products are relatively lower (0.72 and 0.73, respectively). Compared with ME value (−0.11) of TRMM data, ME values of GPM products (6.47, 6.45, 5.31) are quite different from the optimal ME value. RE and ME of the research product (06F) were slightly closer to optimal value than real-time products (06E, 06 L). This indicates that systematic bias of GPM real-time products was comparatively low and post-processing of research products was less effective. However, the offsetting effect of positive and negative errors resulted in ME of TRMM data close to zero. NMAE of real-time products 06E and 06 L reached about 8% while NRMSE was about 0.7%. NMAE and NRMSE of the research product 06F relatively reduces, with NMAE about 5.8% while NRMSE was lower than 0.6%. As for TRMM data, NMAE and NRMSE are both rather poor (45.8% and 96.9%, respectively). Above all, there was a great improvement of GPM products relative to TRMM.

As for the ability of satellite products to capture precipitation events, Table 5 shows that GPM products have a higher false alarm rate than TRMM. However, the POD values of GPM data are about 0.4 higher than that of TRMM data and HHS values of GPM data are approximately 0.2 higher than that of TRMM data. The above results indicate that, compared with TRMM, the detection ability of GPM for rainfall events increases but the false alarm rate also increases, which is related to the higher spatiotemporal resolution of GPM. Overall, the ability to capture rainfall events of GPM products has improved considerably.

**Table 5** | Values of statistical indices among TRMM, GPM, and GV data

| Index | Unit | Range | Optimum | TRMM | 06E | 06 L | 06F |
|---|---|---|---|---|---|---|---|
| Mean | mm | $[0,+\infty)$ | – | 3.97 | 4.41 | 4.40 | 4.31 |
| CC | – | $[-1,1]$ | 1 | 0.88 | 0.72 | 0.73 | 0.78 |
| NSE | – | $(-\infty, 1]$ | 1 | 0.72 | 0.17 | 0.17 | 0.44 |
| ME | mm | $(-\infty,+\infty)$ | 0 | −0.11 | 6.47 | 6.45 | 5.31 |
| MAE | mm | $[0,+\infty)$ | 0 | 1.82 | 1.59 | 1.58 | 1.30 |
| RMSE | mm | $(-\infty,+\infty)$ | 0 | 3.85 | 0.34 | 0.33 | 0.24 |
| RE | % | [0, 100] | 0 | −2.9 | 2.86 | 2.73 | 2.43 |
| NMAE | % | [0, 100] | 0 | 45.8 | 8.30 | 8.02 | 5.78 |
| NRMSE | % | $[0,+\infty]$ | 0 | 96.9 | 0.70 | 0.67 | 0.60 |
| POD | – | [0, 1] | 1 | 0.47 | 0.75 | 0.75 | 0.78 |
| FAR | – | [0, 1] | 0 | 0.07 | 0.18 | 0.16 | 0.17 |
| HHS | – | [−1, 1] | 1 | 0.41 | 0.59 | 0.62 | 0.62 |
| (1) | (2) | (3) | (4) | (5) | (6) | (7) | (8) |

The indices values are computed by averaged areal precipitation on catchment scale.

Indices of each grid calculated by TRMM, GPM data, and GV data are represented in Figures 3 and 4, respectively. Looking at the perspective of consistency, compared with the real-time products 06E and 06 L, 06F has higher NSE value on each grid. Grids with NSE value under 0 of real-time products occupied the majority of the catchment, while grids with NSE values over 0 of 06F take up the majority of the catchment (seen Figure 4). Looking at the other aspect, RE value in Figure 4 indicate that in low areas, real-time products are more likely to overestimate precipitation than research products. The above two indices uncovered that both real-time products and research products showed that NSE was higher and tended to underestimate precipitation at large accumulated rainfall region, indicating that spatial distribution of precipitation estimation accuracy is affected by total rainfall of the region. As for the ability to capture rainfall events, POD and FAR of GPM products tended to be higher in the north and lower in the southern area of the study region, indicating that false alarm rate had a tendency to be higher where there are high detection rates.

Figure 4 compares the accuracy of different GPM products in different spatial scales. All indices of GPM products under catchment scale precede those of grid scale and the accuracy of precipitation estimates varies from grid to grid. According to precision comparison results of different GPM products, accuracy of 06E and 06 L is very similar, but not all index values of the research product are superior to those of real-time products. This scenario reveals that the new version of research products (06F) is not absolutely better than the real-time products, manifested in the following aspects:

1. The results of consistency (CC) and relative error (RE) of GPM data and GV data show that the research product (06F) performed better than the real-time products (06E, 06 L).
2. In terms of the ability to detect rainfall events, TRMM shows the worst performance in POD among four sets of products, but then, FAR is the optimum.

#### 4.1.3. Investigation of GPM data under different temporal scale

In order to evaluate the accuracy of GPM data under different temporal scales, this study calculates the statistical indices in monthly scale. The values of CC and NSE in Figure 5(a) illustrate that GPM data performed better in the wet season than in the dry season, and the consistency between real-time products and GV data is particularly poor in January. Figure 5(a) also shows a significant improvement in the monthly NSE value for 06F compared to that of 06E and 06 L. This situation indicates post-processing of GPM is able to gain a decent result on the monthly scale.

For capacity of detecting precipitation events, Figure 5(b) shows the probability of detection (POD) and false alarm ratio (FAR) value of three GPM products, which can be summed up as follows:

1. POD indicates GPM products tended to capture rainfall events in the warm season (from May to October) and miss rainfall events in the cold season (from January to April, from November to December) and this phenomenon is particularly obvious in winter.
2. The indices of GPM show unobvious regularity in dry and wet periods. Compared with the real-time product, the research product mainly reduces the degree of overestimate and underestimate deviation, but neither POD nor FAR of 06F improves, compared with 06E and 06 L. To some extent, it indicates post-processing of 06F made hardly any further enhancements in temporal scale.

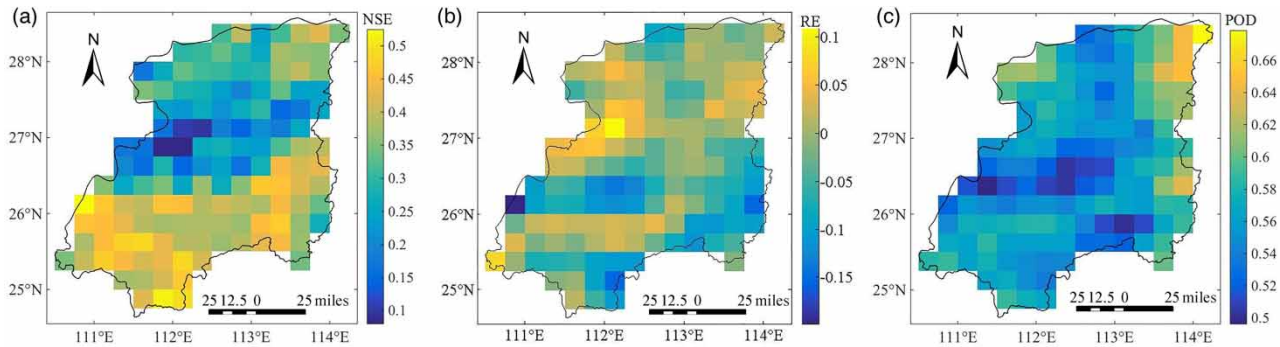


**Figure 3** | The spatial distributions of (a) NSE, (b) RE, and (c) POD. All the indices are calculated based on daily TRMM and GV precipitation datasets from 2006 to 2014 (Wang *et al.* 2018).

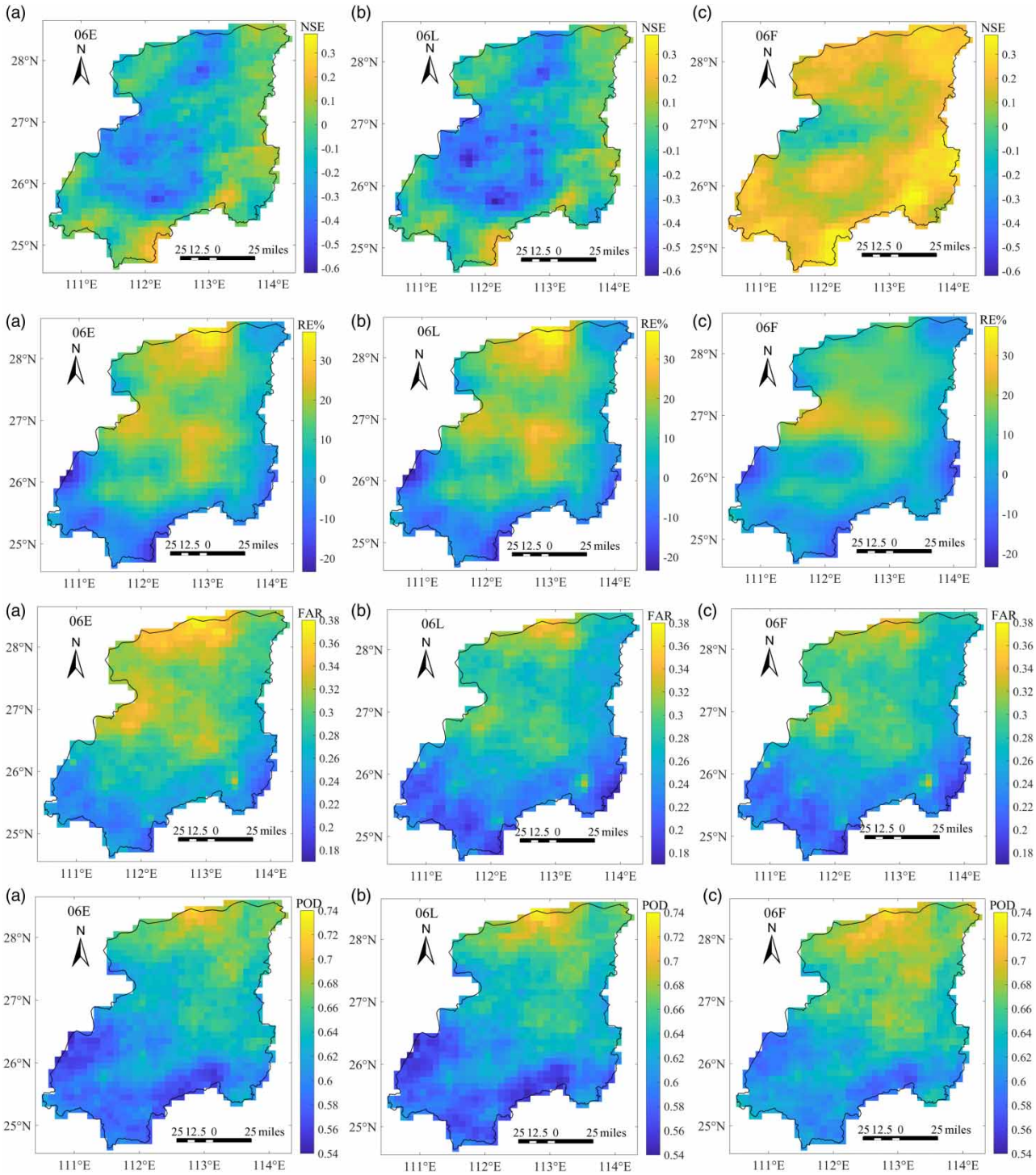


**Figure 4** | Spatial distribution of indices, values of each index were calculated from daily rainfall GPM data and GV data of 909 grids in the catchment during the period of 2006–2018.

### 4.2. Estimation of extreme precipitation from satellite product data

In order to evaluate the capacity of satellite products catching extreme precipitation events under catchment scale, this study calculates several indices for extreme rainfall assessment.

Figure 6 displays estimation of extreme rainfall under 909 GPM grids, which can be summarized as follows:

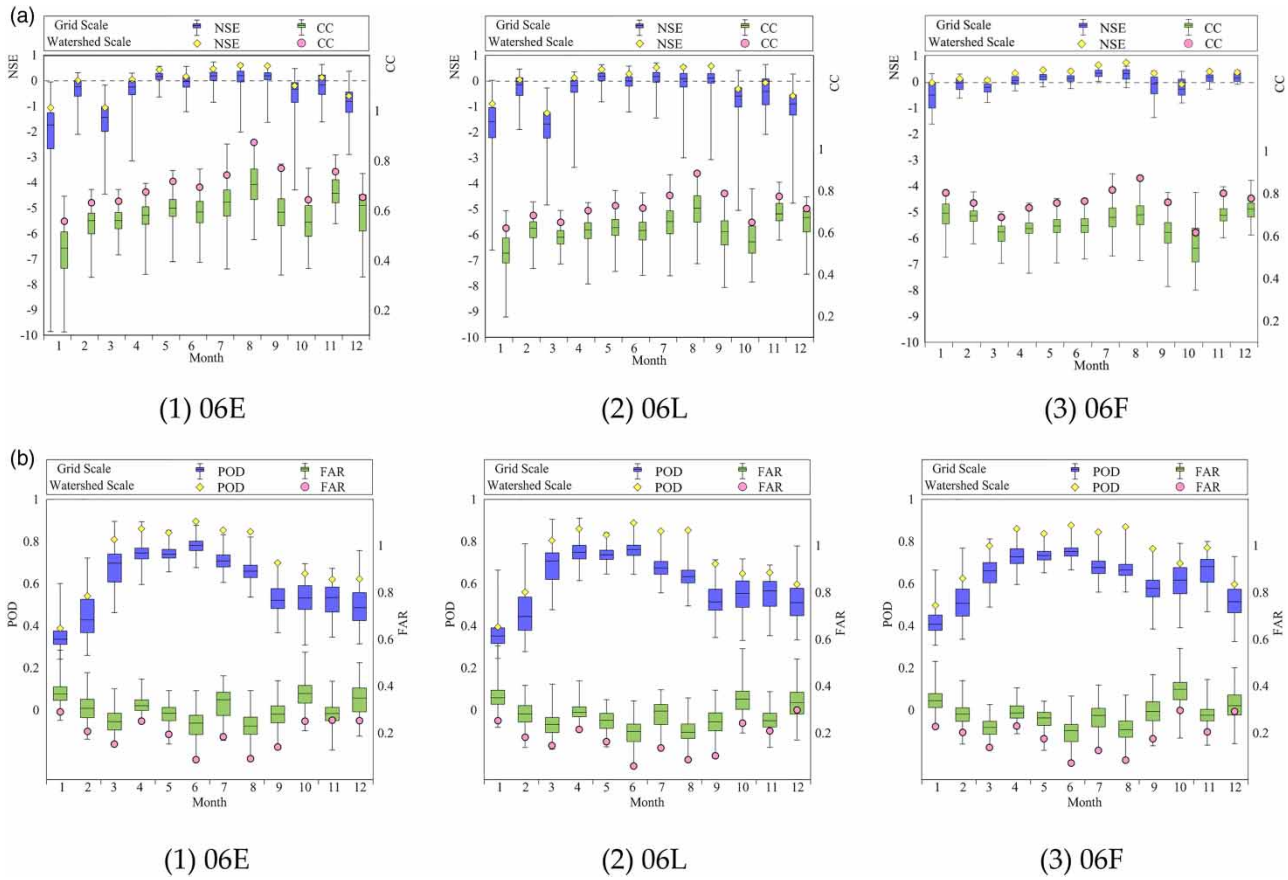


**Figure 5** | (a) Box plots of NSE and CC of GPM data for different months (2006–2018). ◇ and ○ are catchment-scaled indices, and the box plots are indices at grid scale containing 909 grid indices in Xiangjiang river catchment (boxes indicate the first (q25) and the third (q75) quartiles, and the black horizontal line indicates the minimum, median, and maximum). Indicators are computed by using daily precipitation data of GPM data and GV data monthly. (b) Box plots of POD and FAR of GPM data for different months (2006–2018). ◇ and ○ are catchment-scaled indices, and the box plots are indices at grid scale containing 909 grid indices in Xiangjiang river catchment (boxes indicate the first (q25) and the third (q75) quartiles, and the black horizontal line indicates the minimum, median, and maximum). Indicators are computed by using daily precipitation data of GPM data and GV data for every month.

1. First, GPM is liable to overestimate the number of days that rainfall amount exceeded 20 mm/d. Second, GPM products tend to overestimate maximum continuous dry days but underestimate maximum continuous wet days, among which, underestimation of 06F is particularly evident.
2. As for the estimation of maximum precipitation, catchment and grid scale results of P99, P1d, and P5d show that GPM tends to overestimate maximum rainfall. Real-time products overvalue precipitation more compared with research product 06F.

### 4.3. Spatiotemporal variation of error components

#### 4.3.1. Error decomposition of GPM

According to the incidence rate of error components, HBIAS accounted for the largest proportion of total error (about 50%), the proportion of MBIAS is less than 30%, and FBIAS occupied the minimum percentage of occurrence. In relation to error contribution rate, HBIAS of 06E, 06 L, and 06F provided 9.5%, 11.7%, and 8.6%, respectively (Table 6), estimation error (HBIAS) resulted in overestimates of precipitation while MBIAS led to precipitation being undervalued. Figure 7 demonstrates that effect of accumulated rainfall was apparent in Xiangjiang catchment, in addition, with enrichment of accumulated precipitation, total error TBIAS showed a trend from positive bias to negative bias which was dominated by HBIAS and MBIAS. Improvement of research product relative to real-time products is to reduce overestimation of

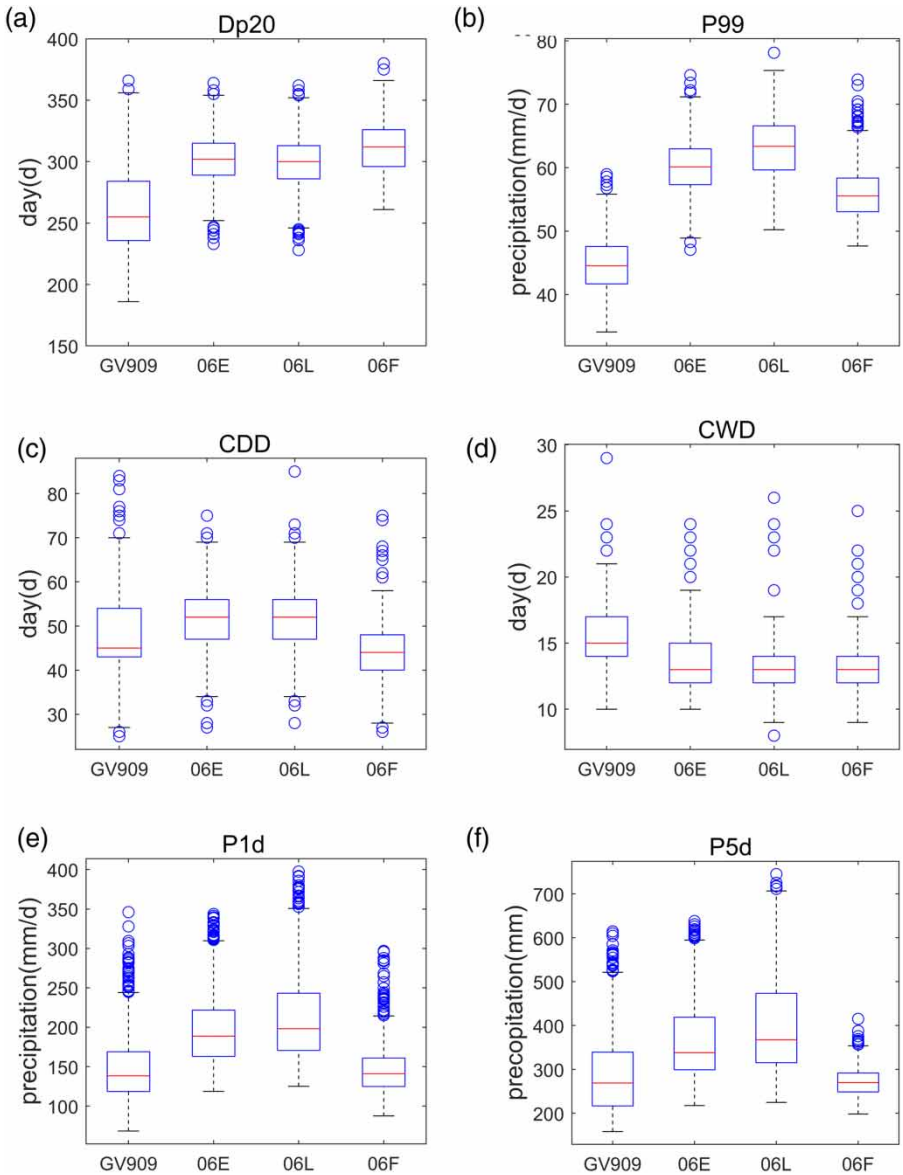


**Figure 6** | Boxplot of extreme rainfall assessment index values of three GPM products and GV data.

**Table 6** | Error components of different GPM products

| | Occurrence proportion | | | Contribution percentage | | |
|---|---|---|---|---|---|---|
| | 06E | 06L | 06F | 06E | 06L | 06F |
| HBIAS | 49.8 | 50.9 | 51.9 | 9.5 | 11.7 | 8.6 |
| MBIAS | 30.2 | 31 | 29.2 | −17.5 | −17.5 | −16.4 |
| FBIAS | 20.1 | 18.1 | 18.8 | 16.8 | 14.3 | 14 |
| TBIAS | 100 | 100 | 100 | 8.9 | 8.5 | 6.2 |

HBIAS. However, post-processing aggravated the overestimation degree of FBIAS at the same time. Moreover, there is no obvious development on MBIAS between the two types of product. In summary, different error components of GPM had an offset effect on each other and the total error between GPM and the rain gauge appear to be smaller than the actual error.

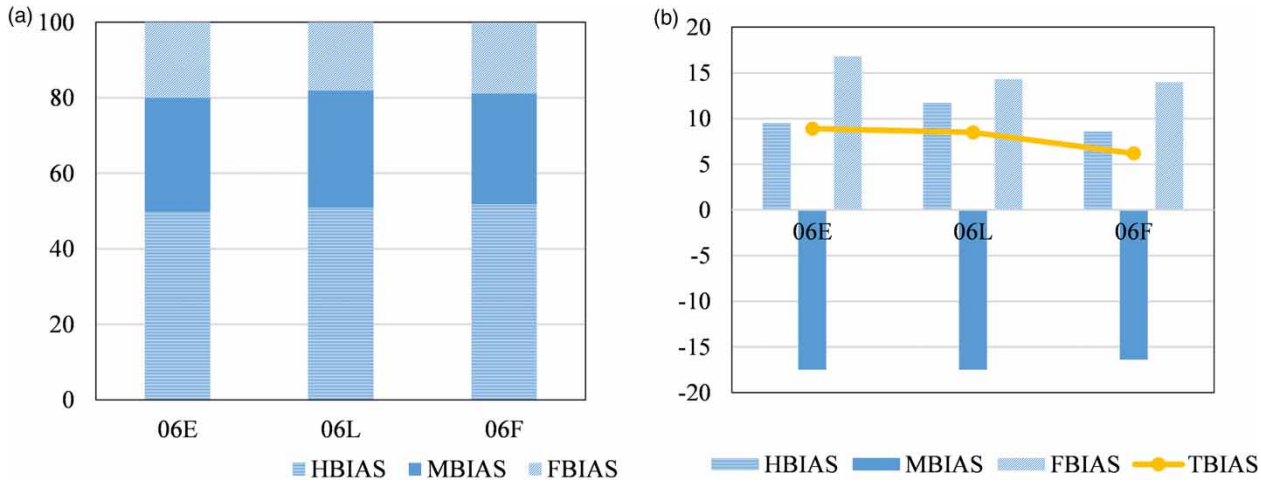


**Figure 7** | Error components of three GPM products: (a) occurrence proportion of error components; (b) contribution percentage of HBIAS, MBIAS, FBIAS and TBIAS.

The spatial distribution of error components and total error of real-time products 06E, 06 L, and research product 06F are shown in Figure 8. Outcomes can be summed up as two aspects:

1. Error spatial distribution of real-time products is similar to those of research products; nonetheless, research products' cumulative amount of each error component has been reduced.
2. Estimation error HBIAS and omission error MBIAS were dominant components affecting the spatial distribution of total error TBIAS and their error distribution was similar to the spatial distribution pattern of total rainfall (see Figure 3). A pattern emerged that regions with higher precipitation tended to have aggravated negative bias and decreased positive bias.

#### 4.3.2. Cause analysis of spatiotemporal variation based on error components method

As stated in the above research, the precision of satellite rainfall data was influenced by season, and it was also affected by topography and annual rainfall in space scale. This is due to the reason that topography is mainly related to elevation while precipitation distribution and total amount of different seasons depends on rainfall occurrence frequency and rainfall intensity distribution. Thus, spatial and temporal diversity in satellite data accuracy is mainly attributed to three influencing factors, elevation, total rainfall amount, and rainfall intensity.

According to China Meteorological Administration, daily precipitation intensities were classified into four levels (Table 7).

Table 8 shows the error distribution of misreported rainfall events and unreported rainfall events under different rainfall intensities in GPM data, according to results, with increase of rainfall intensity, incidence rate and proportion of FBIAS and MBIAS declined. In general, low-intensity rainfall took up the dominant part in the omission and misreporting of rainfall, while that of high-intensity rainfall (such as heavy rain and rainstorm) occupied a small proportion.

The results in Table 8 reveal that two main factors influencing the accuracy of GPM are the total amount of precipitation and precipitation intensity. As discussed before, little rain tended to be overestimated, in the meantime, omission and false alarm also happened more frequently in low-intensity rainfall events (precipitation between 1 and 10 mm/d). Consequently, low-intensity rainfall events mainly brought about positive skewed HBIAS and FBIAS, but negative skewed MBIAS. In addition, higher-intensity precipitation led to a stronger negative skewed HBIAS.

## 5. CONCLUSIONS

To assess and develop satellite precipitation products such as TRMM and GPM has become a diligent direction of researchers. Error sources tracing and causes analyzing of spatiotemporal variation can provide a basis for improving precipitation data accuracy, thus allowing hydrologic simulation to be more efficient by providing a relatively reliable data input. In this

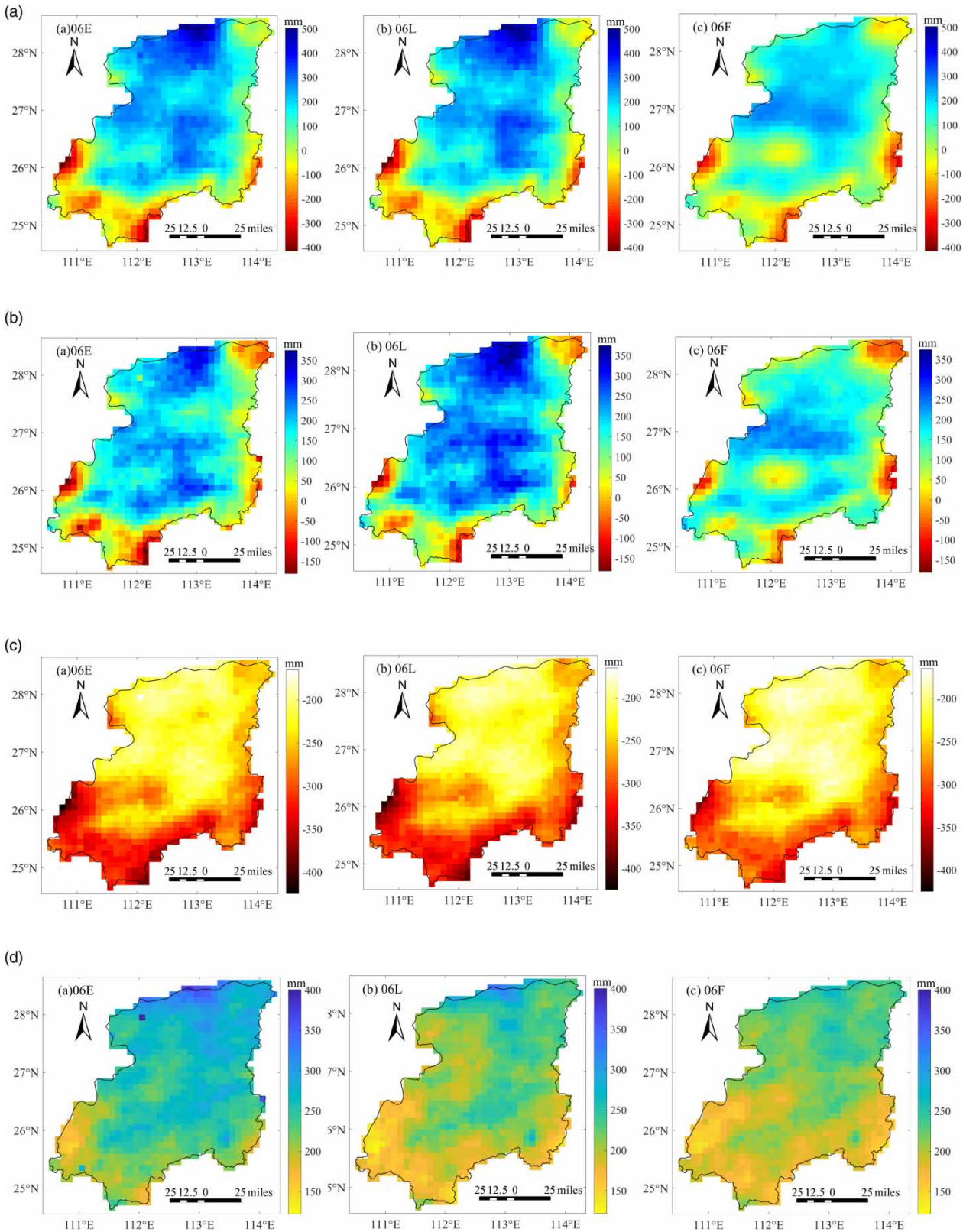


**Figure 8** | Spatial distribution of error components of different GPM products and cumulative amount of total error during the research period March 2006–December 2018: (a) TBIAS, (b) HBIAS, (c) MBIAS, and (d) FBIAS.

**Table 7** | Precipitation intensity classification

| Grade | Classification | Precipitation intensity (mm/d) |
|---|---|---|
| I | Light rain | 1–10 |
| II | Moderate rain | 10–25 |
| III | Heavy rain | 25–50 |
| IV | Rainstorm | >50 |

The classification basis of precipitation intensity can be found on the website: http://www.cma.gov.cn.

**Table 8** | Influence of rainfall intensity on error decomposition

| | P0 | P10 | P25 | P50 | P100 |
|---|---|---|---|---|---|
| 06 L | | | | | |
| HBIAS | 0 | 88.780 | 9.640 | 1.359 | 0.221 |
| MBIAS | 0.002 | 83.234 | 11.358 | 3.791 | 1.615 |
| FBIAS | 0 | 54.767 | 30.365 | 11.869 | 2.999 |
| TBIAS | 0.001 | 57.123 | 24.669 | 11.957 | 6.249 |
| **06F** | | | | | |
| HBIAS | 0 | 89.102 | 9.280 | 1.395 | 0.223 |
| MBIAS | 0.002 | 83.733 | 11.359 | 3.905 | 1.001 |
| FBIAS | 0 | 55.586 | 29.958 | 11.540 | 2.916 |
| **06E** | | | | | |
| HBIAS | 0 | 88.641 | 9.874 | 1.283 | 0.202 |
| MBIAS | 0.018 | 81.739 | 12.960 | 3.883 | 1.399 |
| FBIAS | 0 | 54.935 | 30.172 | 11.889 | 3.004 |

study, spatiotemporal differences of GPM data are illustrated through the following aspects: initially, the accuracy of GPM (06E, 06 L, and 06F) products was appraised by calculating bias between satellite-based data and rain gauge data of Xiangjiang river catchment. In order to track error source, total errors of satellite precipitation data were divided into hit bias (HBIAS: precipitation detected by both GPM and rain gauge station), missed precipitation (MBIAS: precipitation detected only by rain gauge station), and false precipitation (FBIAS: precipitation detected only by GPM) accordingly. Subsequently, the impact of precipitation intensity and total precipitation on the accuracy of GPM data and their influence on three error components were evaluated. The main results of this study are as follows:

1. Both TRMM and GPM data show a better performance on larger spatiotemporal scale and perform quite poorly in estimating extreme precipitation in either magnitude or time range. In the rainy season, measured accurateness of satellite precipitation data is higher. Moreover, in winter and mountainous regions, GPM data tend to show an underestimation on precipitation.
2. Compared to TRMM, the accuracy of GPM has improved. However, the improvement of GPM research products relative to its real-time products is only reflected in the accuracy of precipitation amount estimation, and the ability of precipitation event detection remains to be further enhanced. The accuracy of TRMM and GPM data reveals significant spatiotemporal transformations under the influence of season, precipitation intensity, and total precipitation.
3. Results of the proportion of each error component under different precipitation intensity show that rainfall intensity significantly affects the accuracy of GPM. Under low precipitation intensity circumstance, omission and false alarm of precipitation events tend to occur. According to the results of HBIAS, GPM has a tendency to overestimate low-intensity precipitation, whereas it tends to underestimate high-intensity precipitation. In addition, with the growth of precipitation

intensity, the negative component of daily hit bias increases. The combination of precipitation events of different intensity directly affects the total amount of precipitation, and the cumulative amounts and occurrence frequency of different error components are spatially affected by the total precipitation.

4. The spatiotemporal distribution differences of satellite precipitation data mainly comes from the change of detection ability of satellite products due to season and precipitation intensity. In winter, the foremost factor triggering underestimation of GPM is omission of precipitation events, which is due to a poor capability of satellite products to catch small rain events. In terms of the negative error of GPM data, the greater the frequency and intensity of high-intensity precipitation, the larger the negative component of hit bias. Additionally, the increasing number of rainy days and missed events increases negative error. These may explain why a bigger negative error arises in grids or days with large amounts of total precipitation.

In general, versions and algorithms of satellite precipitation products are still being updated constantly. Its application potential and its future development prospects in data-deficit areas are worth exploring. Comprehensive accuracy assessment will help to provide a reference for product users and for algorithm improvement, while error analysis and discussions on causes of spatiotemporal variation will help to extend understanding of the impact of climate, rain intensity, and other factors on the accuracy of GPM products. To some extent, it can help to explain the root causes of spatial and temporal accuracy differences in different regions. These analyses are a benefit for tracking error sources and guiding the direction of GPM product improvement. Hence, error sources tracking analysis will facilitate improving the accuracy of precipitation measurement for satellite products and that will provide a higher quality data source for subsequent studies.

## AUTHOR CONTRIBUTIONS

Conceptualization, B.T. and H.C.; methodology, B.T and J.W.; validation, B.T., H.C., and C.X.; formal analysis, B.T.; investigation, B.T. and J.W.; writing – original draft preparation, B.T.; writing – review and editing, H.C. and B.T. All authors have read and agreed to the published version of the manuscript.

## CONFLICTS OF INTEREST

The authors declare no conflicts of interest.

## FUNDING

This research was funded by National Key Research and Development Program (2017YFA0603702).

## DATA AVAILABILITY STATEMENT

All relevant data are available from an online repository or repositories (https://pmm.nasa.gov/data-access/downloads/trmm; https://pmm.nasa.gov/data-access/downloads/gpm; http://www.gscloud.cn).

## REFERENCES

Adam, M., Racha, E. & Michael, D. 2015 Assessment and comparison of TMPA satellite precipitation products in varying climatic and topographic regimes in Morocco. *Remote Sensing* **7** (5), 5697–5717.

Adhikary, S. K., Yilmaz, A. G. & Muttil, N. 2015 Optimal design of rain gauge network in the Middle Yarra River catchment, Australia. *Hydrological Processes* **29** (11), 2582–2599.

Basistha, A., Arya, D. S. & Goel, N. K. 2008 Spatial distribution of rainfall in Indian Himalayas – a case study of Uttarakhand Region. *Water Resources Management* **22** (10), 1325–1346.

Cai, Y., Jin, C., Wang, A., Guan, D., Wu, J., Yuan, F. & Xu, L. 2015 Spatio-temporal analysis of the accuracy of tropical multisatellite precipitation analysis 3B42 precipitation data in mid-high latitudes of China. *Plos One* **10** (4), e0120026. doi:10.1371/journal.pone.0120026.

Camera, C., Bruggeman, A., Hadjinicolaou, P., Pashiardis, S. & Lange, M. A. 2014 Evaluation of interpolation techniques for the creation of gridded daily precipitation (1 × 1 km2); Cyprus, 1980–2010. *Journal of Geophysical Research Atmospheres* **119** (2), 693–712.

Chen, S., Hong, Y., Cao, Q., Gourley, J. J., Kirstetter, P. E., Yong, B., Tian, Y., Zhang, Z., Shen, Y. & Hu, J. 2013a Similarity and difference of the two successive V6 and V7 TRMM multisatellite precipitation analysis performance over China. *Journal of Geophysical Research Atmospheres* **118** (23), 13060–013074.

Chen, S., Hong, Y., Gourley, J. J., Huffman, G. J., Tian, Y., Cao, Q., Yong, B., Kirstetter, P. E., Hu, J. & Hardy, J. 2013b Evaluation of the successive V6 and V7 TRMM multisatellite precipitation analysis over the Continental United States. *Water Resources Research* **49** (12), 8174–8186.

Ebert, E. E., Janowiak, J. E. & Kidd, C. 2007 Comparison of near-real-time precipitation estimates from satellite observations. *Bulletin of the American Meteorological Society* **88** (1), 47–64.

Foehn, A., Hernández, J., Schaefli, B. & Cesare, G. D. 2018 Spatial interpolation of precipitation from multiple rain gauge networks and weather radar data for operational applications in Alpine catchments. *Journal of Hydrology* **563**, 1092–1110.

Germann, U., Galli, G., Boscacci, M. & Bolliger, M. 2010 Radar precipitation measurement in a mountainous region. *Quarterly Journal of the Royal Meteorological Society* **132** (618), 1669–1692.

Haggag, M., Elsayed, A. A. & Awadallah, A. G. 2016 Evaluation of rain gauge network in arid regions using geostatistical approach: case study in northern Oman. *Arabian Journal of Geosciences* **9** (9), 552.

Huffman, G. J., Bolvin, D. T., Nelkin, E. J., Wolff, D. B., Adler, R. F., Gu, G., Hong, Y., Bowman, K. P. & Stocker, E. F. 2010 The TRMM Multisatellite Precipitation Analysis (TMPA): Quasi-global, multiyear, combined-sensor precipitation estimates at fine scales. *Journal of Hydrometeorology* **8** (1), 38–55.

Hyvarinen, O. 2013 A probabilistic derivation of Heidke skill score. *Weather and Forecasting* **29** (1), 177–181.

Kidd, C. 2010 Satellite rainfall climatology: a review. *International Journal of Climatology* **21** (9), 1041–1066.

Krajewski, W. F. & Smith, J. A. 2002 Radar hydrology: rainfall estimation. *Advances in Water Resources* **25** (8/12), 1387–1394.

Krige, D. G. 1951 A statistical approach to some basic mine valuation problems on the Witwatersrand. *Journal of the South African Institute of Mining and Metallurgy* **52**, 119–139.

Lopez, M. G., Wennerström, H., Nordén, L. E. & Seibert, J. 2015 Location and density of rain gauges for the estimation of spatial varying precipitation. *Geografiska Annaler* **97** (1), 167–179.

Ly, S., Charles, C. & Degré, A. 2011 Geostatistical interpolation of daily rainfall at catchment scale: the use of several variogram models in the Ourthe and Ambleve catchments, Belgium. *Hydrology and Earth System Sciences* **15** (7), 2259–2274.

Meischner, P., Collier, C., Illingworth, A., Joss, J. & Randeu, W. 1997 Advanced weather radar system in Europe: the COST 75 Action. *Bulletin of the American Meteorological Society* **78** (7), 1411–1430.

Mishra, A. K. & Coulibaly, P. 2009 Developments in hydrometric network design: a review. *Reviews of Geophysics* **47** (2), 2415–2440.

Moazami, S., Golian, S., Kavianpour, M. R. & Hong, Y. 2013 Comparison of PERSIANN and V7 TRMM Multi-satellite Precipitation Analysis (TMPA) products with rain gauge data over Iran. *International Journal of Remote Sensing* **34** (22), 8156–8171.

Pari, S., Katiraie, B., Nasrin, N., Hsu, K. & Sorooshian, S. 2013 Evaluation of satellite-based precipitation estimation over Iran. *Journal of Arid Environments* **97** (12), 205–219.

Pipunic, R. C., Ryu, D., Costelloe, J. F. & Su, C.-H. 2015 An evaluation and regional error modeling methodology for near-real-time satellite rainfall data over Australia. *Journal of Geophysical Research Atmospheres* **120** (3), 135–141.

Sauvageot, H. 1994 Rainfall measurement by radar: a review. *Atmospheric Research* **35** (1), 27–54.

Tian, Y., Peters-Lidard, C. D., Eylander, J. B., Joyce, R. J., Huffman, G. J., Adler, R. F., Hsu, K. L., Turk, F. J. & Zeng, J. 2009 Component analysis of errors in satellite-based precipitation estimates. *Journal of Geophysical Research Atmospheres* **114**, D24.

Wang, J., Chen, H., Xu, C.-Y., Zeng, Q., Wang, Q., Kim, J.-S., Chen, J. & Guo, S. 2018 Tracking the error sources of spatiotemporal differences in TRMM accuracy using error decomposition method. *Hydrology Research* **49** (6), 1960–1976.

Wilks, D. S. 2006 Statistical methods in the atmospheric sciences, Vol. 100. *Publications of the American Statistical Association* **102** (477), 380.

Yong, B., Chen, B., Tian, Y., Yu, Z. & Hong, Y. 2016 Error-component analysis of TRMM-based multi-satellite precipitation estimates over mainland China. *Remote Sensing* **8** (5), 440.

Zhang, X., Alexander, L., Hegerl, G. C., Jones, P., Tank, A. K., Peterson, T. C., Trewin, B. & Zwiers, F. W. 2011 Indices for monitoring changes in extremes based on daily temperature and precipitation data. *Wiley Interdisciplinary Reviews Climate Change* **2** (6), 851–870.

Zulkafli, Z., Buytaert, W., Onof, C., Manz, B., Tarnavsky, E., Lavado, W. & Guyot, J. L. 2014 A comparative performance analysis of TRMM 3B42 (TMPA) versions 6 and 7 for hydrological applications over Andean-Amazon River Basins. *Journal of Hydrometeorology* **15** (2), 581–592.

First received 28 December 2020; accepted in revised form 9 July 2021. Available online 9 September 2021